

Journal of Mechanics of Materials and Structures

**GRADIENT-ENHANCED LARGE STRAIN THERMOPLASTICITY WITH
AUTOMATIC LINEARIZATION AND LOCALIZATION SIMULATIONS**

Jerzy Pamin, Balbina Weisło and Katarzyna Kowalczyk-Gajewska

Volume 12, No. 1

January 2017



GRADIENT-ENHANCED LARGE STRAIN THERMOPLASTICITY WITH AUTOMATIC LINEARIZATION AND LOCALIZATION SIMULATIONS

JERZY PAMIN, BALBINA WCISŁO AND KATARZYNA KOWALCZYK-GAJEWSKA

The paper deals with the thermomechanical extension of a large strain hyperelasto-plasticity model and focuses on algorithmic aspects and localization simulations. The formulation includes the degradation of the yield strength due to the increase of an averaged plastic strain measure and temperature, thus, three sources for loss of stability are included in the description. A gradient-enhancement of the model is incorporated through an additional differential equation, but localization is also influenced by heat conduction. The finite element analysis is performed for an elongated plate in plane strain conditions, using different finite elements and values of material parameters related to regularization (internal length scales are related to gradient averaging as well as heat conduction). In particular, the influence of the F -bar enrichment on the simulation results is studied. All computational tests are performed using self-programmed user subroutines prepared within a symbolic-numerical tool *AceGen* which is equipped with automatic differentiation options, allowing for automatic linearization of the governing equations.

1. Introduction

The research presented in this paper is focused on the development of a gradient-enhanced geometrically nonlinear thermoplasticity model and its numerical analysis with special attention paid to simulation of strain localization caused by material, thermal and geometrical softening. The phenomenon of localization, in which deformation concentrates in narrow bands whereas the rest of the material specimen experiences unloading, is closely connected with the notion of material instability, the theoretical basis of which goes back to [Hill 1958; Thomas 1961; Rice 1976]. Significant contributions to the subject of numerical simulation of instability and strain localization for isothermal conditions were offered among others in [Rudnicki and Rice 1975; Belytschko and Lasry 1989; de Borst et al. 1993; Sluys 1992; Vardoulakis and Sulem 1995; Tvergaard 1999; Menzel 2002; Forest and Lorentz 2004; Bigoni 2012; Benallal and Marigo 2007]. On the other hand, thermomechanical coupling in the instability analysis was discussed for instance in [Abeyaratne and Knowles 1999; Dunwoody and Ogden 2002; Rooney and Bechtel 2004] (thermoelasticity), [Duszek et al. 1992; Steinmann et al. 1999] (thermoplasticity under the assumption of adiabatic conditions) and [Benallal and Bigoni 2004] (analysis including heat conduction in thermoelastic materials).

If a constitutive model includes material softening, regularization is required to prevent the governing equations from the loss of ellipticity and the simulation results from pathological mesh-dependence. In a thermomechanical problem a gradient-enhancement can be applied in two ways: as an introduction

Contract/grant sponsor: National Science Centre of Poland 2014/15/B/ST8/01322.

Keywords: thermoplasticity, softening, gradient averaging, strain localization, automatic linearization, *AceGen* package.

of higher order gradients of a mechanical field in the material description, e.g., gradient plasticity [Belytschko and Lasry 1989; Zbib and Aifantis 1988a; 1988b; 1988c; de Borst and Mühlhaus 1992] and gradient damage [Pijaudier-Cabot and Bažant 1987; Steinmann 1999], or as an incorporation of higher order gradients of a temperature field (spatial or time derivatives) in, for example, the energy balance or heat conduction equation [Müller and Ruggeri 1993; Aifantis 1992; Forest and Aifantis 2010]. It is worth mentioning at this point that already in book [Eringen 1967] incorporation of higher order gradients of displacements and temperature in the constitutive description is admitted. In the cited book, a material is called simple if mechanical and thermal grades are equal to one: $G(1,1)$. The regularizing influence of heat conduction is discussed in several papers, e.g., in [LeMonds and Needleman 1986] or [Batra and Kim 1991] and publications cited therein.

The mechanical part of the presented model is based on the constitutive description introduced in [Geers 2004], which involves hyperelasto-plasticity with degradation of yield strength via a damage-like variable. However, combinations of plasticity with continuum damage can also be considered, e.g., [Areias et al. 2003] or [Wcisło et al. 2013]. The analysis of fully coupled thermoplasticity models in the thermodynamic framework, which is the basis for the development of the isothermal description, can be found in the papers by Simo, Miehe, Ortiz or Ristinmaa and their coworkers, e.g., [Simo and Miehe 1992; Simo and Hughes 1998; Yang et al. 2006; Ristinmaa et al. 2007].

The research presented in this paper is limited to phenomenological continuum modeling with the following assumptions: initial isotropy of the material, hyperelasticity, rate independent plasticity with associated flow rule, strain hardening with one internal variable and degradation of the yield strength due to the increase of temperature and of a plastic strain measure. However, the description can easily be extended to more elaborated models of plasticity. Furthermore, the thermal part of the formulation makes use of Fourier's law applied to the nonstationary heat flow. All models are developed in a three-dimensional space.

One of the aspects discussed in the paper is the application of symbolic-numerical *Ace* packages [Korelc 2011] as convenient tools for the implementation of complex models and their numerical verification. In this paper, all tests are performed using self-programmed user subroutines. In particular, an elongated plate in a plane strain regime is simulated using different finite elements and material parameters influencing the width of the localization band. The numerical analysis is focused on the following issues:

- the influence of finite element enhancement *F-bar* designed to prevent volumetric locking for volume preserving plasticity, and
- examination of the model response in the presence of gradient regularization, heat conduction and a combination of the two.

The research reveals that in the analyzed case of a tensioned plate, the application of the *F-bar* finite element enhancement influences the results only in the post peak regime, but the application of elements without enrichment can even preclude the shear band formation. Moreover, although both types of regularization (gradient-enhancement and heat conduction) influence the mesh-dependence of the results and the ductility of the material response, they produce different forms of deformation.

The paper is laid out as follows. The computational strategy adopted for the analyzed model is discussed in Section 2. In particular, the application of the symbolic-numerical tools is justified and a general

procedure used for the finite element user subroutine is presented. Section 3 deals with the constitutive relations for the gradient-enhanced thermomechanical model of hyperelasto-plasticity. Moreover, three governing equations (the balance of linear momentum, the balance of energy and the averaging equation) are presented in their strong form alongside their corresponding weak formulations. Section 4 contains a concise discussion outlining the finite element implementation of the presented coupled model within *Ace* packages. The results of the numerical simulations are presented in Section 5. This section is divided into two parts: first, the isothermal model is tested for different finite elements and internal length scales, next the results for the thermomechanical model are included. The attention is focused mainly on the influence of the internal length scale introduced by gradient averaging and heat conduction as well as on the behavior of the sample when two localization limiters are applied simultaneously. The paper ends with concluding remarks.

2. Computational strategy

The constitutive model presented in the paper includes two sources of nonlinearities: geometrical (due to large deformations) and material (plasticity). Next, the gradient enhancement is adopted, which requires solving an additional averaging equation. Eventually, the full thermomechanical coupling is taken into account. All those issues produce a highly complex problem which can only be solved using user-programmed routines for a chosen solver.

To find the solution to the nonlinear problem within the Finite Element Method (FEM), the standard Newton–Raphson procedure is used, which guarantees the quadratic convergence of the computations. However, this method requires derivation of the consistent tangent matrix on the basis of linearized governing equations. For such an elaborated model, the analytical derivation of linearization is very difficult or even infeasible. Alternatively, numerical differentiation can be applied, e.g., in [Pérez-Foguet et al. 2000] that method is used for derivation of local (at the Gauss point level) and global tangent operators.

The next step after the formulation of the numerical algorithm is the implementation of the user supplied procedure within a programming language which is required by a selected FEM engine. Usually, standard FEM software relies on Fortran or C languages, which are not very convenient tools for matrix operations. This standard approach also has a significant inconvenience as any modification of the model or its development requires renewed linearization and, hence, reformulation of the numerical procedure.

To focus more on the developed model and on the behavior of the simulated material, instead of the analytical derivations and programming, symbolic-numerical tools have been chosen for the numerical analysis. The packages which are used in this paper are *AceGen* and *AceFEM* [Korelc 2011], which work in the *Wolfram Mathematica* environment. The *AceGen* package is a multilanguage numerical code generator which combines symbolic and algebraic capabilities of *Mathematica*, the automatic differentiation (AD) technique (particularly important if there is a need for linearization) and simultaneous optimization of expressions, which improves efficiency of the generated code. The work with the program includes preparation of the code in a specific symbolic metalanguage based on the notation of *Wolfram Mathematica* and generation of the code in a selected programming language (e.g., C, Fortran or Matlab). In particular, the package supports several FEM environments, such as *Abaqus* or *FEAP*, and also the *AceFEM* package which has been selected by the authors to perform the numerical tests. Although another FEM program could also be used, application of this engine guarantees full control of

simulations due to close collaboration between packages. The important advantage of package *AceGen* is the possibility of relatively easy modifications of the model, as the tangent matrix is derived automatically by the code generator.

The general approach to the solution of a problem using *AceGen* and *AceFEM* package is as follows. First, the unknown field interpolation for a selected finite element has to be introduced,

$$\mathbf{d} = \mathbf{N}_I \cdot \mathbf{p}, \quad (2-1)$$

where \mathbf{p} is a vector of nodal unknowns and \mathbf{N}_I is a vector of interpolation (shape) functions.

According to the author of the packages, the most convenient and effective approach to *Ace* modeling is to define a potential Π for the problem to be solved [Korelc 2008]. Upon the introduction of (2-1) into the functional definition, Π becomes a function of the degrees of freedom \mathbf{p} . Then, for properly formulated dependencies and with the use of Gauss integration, the finite element residual vector for the Newton–Raphson iterative procedure can be automatically computed as

$$\mathbf{R}_{el} = \sum_{nG} w_G J_{XG} \mathbf{R}_G, \quad \mathbf{R}_G = \frac{\partial \Pi}{\partial \mathbf{p}}, \quad (2-2)$$

where nG is the number of Gauss points, w_G is the weight of a Gauss point, J_{XG} is the Jacobian of isoparametric mapping from the parent element to the element in the reference configuration. Accordingly, the tangent operator is derived through the formula

$$\mathbf{K}_{el} = \frac{\partial \mathbf{R}_{el}}{\partial \mathbf{p}}. \quad (2-3)$$

3. Presentation of model

The constitutive description of the isothermal model is based mainly on the paper by Geers [2004]. His model covers large strain hyperelasto-plasticity and can reproduce softening and failure of the material due to an isotropic plastic-damage variable. In this paper, the model is extended to encompass full thermomechanical coupling, including thermal expansion, dependence of the heat flux on deformation, production of heat due to the plastic process and thermal softening, which is understood as degradation of the yield strength with increasing temperature.

3A. Preliminaries and kinematics. To formulate the governing equations, let us introduce the following notation. The continuous body which deforms under an applied load is denoted by \mathcal{B} and has a boundary labeled with $\partial\mathcal{B}$. The referential placement of the body particles at time t_0 is identified with vector \mathbf{X} , and the current position of particle \mathbf{X} at time t is denoted by vector \mathbf{x} .

The movement of the body is described by function $\boldsymbol{\varphi}$ such that $\mathbf{x} = \boldsymbol{\varphi}(\mathbf{X}, t)$. The deformation gradient and its determinant are defined as usual,

$$\mathbf{F} = \frac{\partial \boldsymbol{\varphi}(\mathbf{X}, t)}{\partial \mathbf{X}}, \quad J = \det(\mathbf{F}). \quad (3-1)$$

Next, multiplicative decomposition of the deformation gradient is adopted basing on the concepts applied to elastoplasticity [Lee and Liu 1967; Lee 1969; Mandel 1974; Kroner and Teodosiu 1974] and thermomechanics [Stojanovitch et al. 1964; Lu and Pister 1975; Holzapfel 2000]. Here, the deformation

gradient consists of three parts in order to separate the plastic and elastic deformation as well as thermal expansion,

$$\mathbf{F} = \mathbf{F}^\theta \mathbf{F}^e \mathbf{F}^p. \quad (3-2)$$

Note that the deformation gradient (3-2) can also be formulated in the forms

$$\begin{aligned} \mathbf{F} &= \mathbf{F}^r \mathbf{F}^p = \mathbf{F}^\theta \mathbf{F}^m, \\ \mathbf{F}^r &= \mathbf{F}^\theta \mathbf{F}^e, \\ \mathbf{F}^m &= \mathbf{F}^e \mathbf{F}^p, \end{aligned} \quad (3-3)$$

where \mathbf{F}^r denotes reversible deformation and \mathbf{F}^m the mechanical one. The decomposition (3-2) has been formulated and discussed in [Wcisło and Pamin 2016].

The thermal contribution \mathbf{F}^θ is assumed to be purely volumetric, so for the isotropic material it can be represented as

$$\mathbf{F}^\theta = (J^\theta)^{1/3} \mathbf{I}, \quad J^\theta = \det(\mathbf{F}^\theta), \quad (3-4)$$

where \mathbf{I} is the second order identity tensor, and the deformation caused by a temperature change is determined according to Lu and Pister [1975] as

$$J^\theta = e^{3\alpha_T(T-T_0)}. \quad (3-5)$$

In (3-5), quantities T and T_0 are the absolute temperature and the reference temperature for the stress- and strain-free state, and α_T is the coefficient of linear thermal expansion.

On the basis of the decomposition (3-3) and assumption (3-5), the mechanical part of the deformation gradient can be derived directly as

$$\mathbf{F}^m = e^{-\alpha_T(T-T_0)} \mathbf{F}. \quad (3-6)$$

The consequence of the deformation gradient splitting into the mechanical and thermal parts is the possible application of the algorithm for isothermal elastoplasticity presented in [Wcisło et al. 2013]. Note that in this approach the assumption of volume preserving plasticity is disregarded, contrary to the thermoplastic models presented in [Wriggers et al. 1992; Simo and Miehe 1992; Simo and Hughes 1998].

3B. Free energy function. The state of a material is expressed by the Helmholtz free energy potential, which is assumed in a decoupled form,

$$\psi(\mathbf{b}^e, T, \gamma) = \psi^e(\mathbf{b}^e) + \psi^\theta(T) + \psi^p(\gamma), \quad (3-7)$$

where the first part $\psi^e(\mathbf{b}^e)$ is related to the elastic response and includes thermomechanical coupling responsible for thermal expansion, $\psi^\theta(T)$ is a purely thermal part and, finally, the term $\psi^p(\gamma)$ denotes the potential of isotropic strain hardening in plasticity. In (3-7) $\mathbf{b}^e = \mathbf{F}^e(\mathbf{F}^e)^T$ denotes the elastic left Cauchy–Green tensor and γ is a scalar plastic strain measure. Note that tensor \mathbf{b}^e , computed from \mathbf{F}^e , depends on thermal expansion as presented in the third equation of (3-3) and relation (3-6).

In particular, the parts of the free energy potential are assumed in the subsequent analysis as follows [Simo and Hughes 1998; Miehe 1995]:

$$\psi^e(\mathbf{b}^e) = \frac{1}{2}G(\text{tr}(J_{be}^{-1/3}\mathbf{b}^e) - 3) + \frac{1}{2}K\left(\frac{1}{2}(J_{be} - 1) + \frac{1}{2}\log J_{be}\right), \quad (3-8)$$

$$\psi^\theta(T) = c((T - T_0) - T \ln(T/T_0)), \quad (3-9)$$

$$\psi^p(\gamma) = \frac{1}{2}\sqrt{2/3}h_i\gamma^2 + (\sigma_{y\infty} - \sigma_{y0})\left(\gamma + \frac{1}{\sqrt{2/3}\delta}e^{-\sqrt{2/3}\delta\gamma}\right), \quad (3-10)$$

where G and K are the shear and bulk moduli, J_{be} is the determinant of tensor \mathbf{b}^e , c is the heat capacity at constant deformation, σ_{y0} is the initial yield stress, $\sigma_{y\infty}$ is the residual yield stress, h_i is the linear hardening coefficient whereas δ denotes the saturation parameter which governs the rate of hardening converging to an asymptote: oblique if the linear hardening term is incorporated or horizontal for $h_i = 0$.

In compliance with the second law of thermodynamics (which provides restrictions for the constitutive relations) and the assumed form of the free energy potential (3-7), the state functions of the Kirchhoff stress tensor, entropy and hardening function, are obtained:

$$\boldsymbol{\tau} = 2\frac{\partial\psi}{\partial\mathbf{b}^e}\mathbf{b}^e, \quad \eta = -\frac{\partial\psi}{\partial T}, \quad h = \frac{\partial\psi}{\partial\gamma}. \quad (3-11)$$

The heat capacity can also be derived from the laws of thermodynamics (see [Simo and Miehe 1992] or [Miehe 1995]) as

$$c = -T\frac{\partial^2\psi}{\partial T^2}. \quad (3-12)$$

It can be noticed that for the adopted form of the free energy potential the heat capacity is constant. This is valid only if we assume moderate changes of temperature [Ristinmaa et al. 2007].

3C. Constitutive relations for plasticity. To complete the constitutive description of the problem, the yield condition which governs the plastic regime is defined:

$$F_p(\boldsymbol{\tau}, \gamma, T) = f(\boldsymbol{\tau}) - \sqrt{2/3}\sigma_y(\gamma, T)(1 - \omega_p) \leq 0, \quad (3-13)$$

where $f(\boldsymbol{\tau})$ is a stress measure and $\sigma_y(\gamma, T)$ denotes the evolving yield stress. The analyzed model includes isotropic degradation of the plastic properties of material, so the yield stress is multiplied by factor $(1 - \omega_p)$ depending on the plastic-damage variable ω_p , which varies from 0 for the intact material to 1 for completely damaged material. The evolution of the value of ω_p can be formulated in different ways depending on the analyzed material, see [Geers 2004]. In this paper the following form is applied:

$$\omega_p = 1 - \exp(-\beta\kappa), \quad (3-14)$$

where β is a ductility parameter and κ is a history variable which is assumed here to be equal to $\sqrt{2/3}\gamma$, see [Geers 2004]. Thus, in this model the damage is assumed to begin simultaneously with the plastic process (no damage threshold is considered).

The yield stress appearing in (3-13) is subsequently assumed to include saturation-type strain hardening and linear thermal softening,

$$\sigma_y(\gamma, T) = (\sigma_{y0} + \sqrt{2/3}h_i\gamma + (\sigma_{y\infty} - \sigma_{y0})(1 - e^{-\sqrt{2/3}\delta\gamma}))(1 - h_T(T - T_0)), \quad (3-15)$$

where h_T is the thermal softening modulus. Assuming that $\kappa = \sqrt{2/3}\gamma$, the general formulation presented above can be rewritten as

$$F_p = f(\boldsymbol{\tau}) - \sqrt{2/3}(\sigma_{y0} + \sqrt{2/3}h_i\gamma + (\sigma_{y\infty} - \sigma_{y0})(1 - e^{-\sqrt{2/3}\delta\gamma}))(1 - h_T(T - T_0))e^{-\beta\gamma} \leq 0. \quad (3-16)$$

The adopted stress measure is standard Huber–Mises–Hencky (HMH) definition, which is commonly used to reproduce the behavior of metals, although other measures of stress can be applied as well. The HMH function depends only on the second invariant of the deviatoric Kirchhoff stress tensor, and thus it models volume preserving plasticity.

Following [Simo 1988], the associated flow rule is adopted through the Lie derivative of \mathbf{b}^e ,

$$\frac{1}{2}\mathcal{L}_v\mathbf{b}^e = \dot{\lambda}\mathbf{N}\mathbf{b}^e, \quad (3-17)$$

where $\mathbf{N} = \partial F_p / \partial \boldsymbol{\tau}$ and $\dot{\lambda}$ is the plastic multiplier satisfying the standard Kuhn–Tucker conditions

$$\dot{\lambda} \geq 0, \quad F_p \leq 0, \quad \dot{\lambda}F_p = 0. \quad (3-18)$$

For simplicity we will now limit our considerations to the plastic flow theories for which $\lambda \equiv \gamma$.

3D. Gradient enhancement. As it was mentioned, the model represents a plastic material, which involves a softening behavior and poses difficulties with modeling since the governing equations lose their ellipticity and the boundary valued problem becomes ill-posed [Forest and Lorentz 2004]. To obtain a material model capable of reproducing damage properly, regularization should be applied (e.g., a nonlocal model or higher-order gradient theory selected here) or discontinuous modeling using cohesive elements should be introduced [Li and Chandra 2003].

From the numerical point of view, the loss of well-posedness of the boundary-value problem related to material softening causes mesh-dependence of the results, since the strains tend to localize in the smallest possible volume of the material, which in the finite element model is determined by the size of the element. For that reason, the outcomes for different discretizations do not converge when the mesh is densified and the prediction of the material behavior may be wrong.

To obtain the gradient model, the local variable governing damage, κ , is replaced with its nonlocal counterpart denoted by z , computed using the additional differential equation

$$z - l^2\nabla^2z = \kappa, \quad (3-19)$$

with homogeneous Neumann boundary conditions [Peerlings et al. 2001].

The implicit gradient averaging formulation (3-19) was introduced first in [Peerlings et al. 1996] for a model related to quasibrittle materials. The parameter l appearing in (3-19) is an internal length scale which depends on the adopted material and is often related to its microstructure [Geers et al. 1999].

When the gradient enhancement is applied in the model including large deformations, a configuration to perform the averaging has to be selected [Steinmann 1999]. Here, the material averaging has been adopted on the basis of the analysis included in [Wcisło et al. 2013]. Thus, the gradient in (3-19) is calculated with respect to Lagrangian coordinates and the internal length l is related to the undeformed configuration.

3E. Heat conduction. The constitutive assumption for heat conduction is the classic Fourier law for isotropic materials which is formulated here for the Kirchhoff heat flux vector \mathbf{q} ,

$$\mathbf{q} = -k\nabla T, \quad (3-20)$$

where k is the heat conduction coefficient. The Kirchhoff heat flux is defined in the current configuration. However, it is referred to the area in the undeformed state (it is the Cauchy heat flux multiplied by J [Haupt 2002]). Thus, the temperature gradient ∇T is calculated with respect to Euler coordinates and coefficient k is specified in the reference configuration.

3F. Governing equations and weak forms. The formulation of the problem consists of three governing equations: the linear momentum balance, the internal energy balance and the averaging equation.

3F.1. Linear momentum balance. The linear momentum equation is formulated in the spatial description, yet it is related to the volume of the undeformed body. Following [Simo and Miehe 1992], the local form of the first governing equation is written as

$$\rho_0 \frac{\partial^2 \boldsymbol{\varphi}}{\partial t^2} = J \operatorname{div}(\boldsymbol{\tau}/J) + \rho_0 \mathbf{B}. \quad (3-21)$$

In (3-21), $\operatorname{div}(\cdot)$ is the divergence computed with respect to Eulerian coordinates, ρ_0 is a reference density and \mathbf{B} is a given gravity field. For the static analysis, which is presented in the paper, the left-hand side of (3-21) is equal to zero.

The balance of linear momentum is completed with boundary conditions for displacements \mathbf{u} and tractions \mathbf{t} ,

$$\begin{aligned} \mathbf{u} &= \hat{\mathbf{u}} & \text{on } \partial\mathcal{B}_u, \\ \mathbf{t} &= \boldsymbol{\tau} \cdot \mathbf{n} = \hat{\mathbf{t}} & \text{on } \boldsymbol{\varphi}(\partial\mathcal{B}_\tau), \end{aligned} \quad (3-22)$$

where

$$\partial\mathcal{B}_u \cup \partial\mathcal{B}_\tau = \partial\mathcal{B} \quad \text{and} \quad \partial\mathcal{B}_u \cap \partial\mathcal{B}_\tau = \emptyset. \quad (3-23)$$

The finite element implementation is based on weak forms of the governing equations. Applying the standard derivation (multiplication by test function $\delta\mathbf{u}$, integration over body \mathcal{B} , applying the divergence theorem and Neumann boundary conditions) the balance of linear momentum has the weak form

$$\int_{\mathcal{B}} (\nabla \delta\mathbf{u} : \boldsymbol{\tau} + \delta\mathbf{u} \cdot \mathbf{B}) \, dV + \int_{\boldsymbol{\varphi}(\partial\mathcal{B}_\tau)} \delta\mathbf{u} \cdot \hat{\mathbf{t}} \, da = 0. \quad (3-24)$$

In this paper \mathbf{B} , is assumed to be zero.

3F.2. Energy balance. The second governing equation is the energy balance, which is expressed in the temperature form [Simo and Miehe 1992]

$$c \frac{\partial T}{\partial t} = J \operatorname{div}(-\mathbf{q}/J) + \mathcal{R}, \quad (3-25)$$

where c is the heat capacity at constant deformation and \mathcal{R} is a heat source density which represents heating resulting from plastic dissipation [Wriggers et al. 1992] and is given as

$$\mathcal{R} = \sqrt{2/3} \chi \sigma_y \dot{\gamma}. \quad (3-26)$$

Parameter χ in (3-26) denotes a dissipation heat factor, see [Taylor and Quinney 1934]. The constant value of χ is adopted in this paper for simplicity although consistently with the thermodynamic laws for associated plasticity, its value depends on the initial yield strength and the advancement of the plastic process [Ristinmaa et al. 2007].

Equation (3-25) is completed with appropriate boundary conditions

$$\begin{aligned} T &= \hat{T} & \text{on } \partial\mathcal{B}_T, \\ \mathbf{q} \cdot \mathbf{n} &= \hat{q} & \text{on } \boldsymbol{\varphi}(\partial\mathcal{B}_q), \end{aligned} \quad (3-27)$$

where

$$\partial\mathcal{B}_T \cup \partial\mathcal{B}_q = \partial\mathcal{B} \quad \text{and} \quad \partial\mathcal{B}_T \cap \partial\mathcal{B}_q = \emptyset. \quad (3-28)$$

Note that the essential boundary conditions for \mathbf{u} and T are specified in the reference configuration whereas the natural ones for \mathbf{t} and \mathbf{q} are defined in the current configuration, see [Miehe 1995].

The weak form of the energy balance (3-25) is also obtained using the standard procedure and the backward Euler scheme for time integration. The integral equation valid for the current time is obtained as

$$\int_{\mathcal{B}} \left(\delta T \frac{c}{\Delta t} (T - T_n) + \nabla \delta T k \nabla T - \delta T \mathcal{R} \right) dV + \int_{\boldsymbol{\varphi}(\partial\mathcal{B}_q)} \delta T \hat{q} da = 0, \quad (3-29)$$

where T_n is the value of temperature at the previous time and Δt is the time increment.

3F.3. Averaging equation. The strong form of the averaging equation has already been presented in Section 3D whereas the weak form of the last governing equation needed for FEM implementation after applying the standard procedure is

$$\int_{\mathcal{B}} [(z - \kappa) \delta z + l^2 \nabla_0 z \cdot \nabla_0 \delta z] dV = 0. \quad (3-30)$$

Obviously, equations (3-24), (3-29) and (3-30) must be valid for any admissible weighting functions $\delta \mathbf{u}$, δT and δz .

4. Finite element implementation

This section presents the aspects of implementing the formulated model with symbolic-numerical tools. However, only necessary information is included here as the more in-depth discussion of numerical treatment of other models within Mathematica-based packages *Ace* has already been presented in papers [Wcisło et al. 2013] (gradient damage coupled to plasticity in isothermal conditions), [Wcisło and Pamin 2014; 2016], (entropic thermoelasticity and thermoplasticity with temperature averaging, respectively).

To begin with, the vector of the nodal unknowns of the finite element for the problem includes displacements, temperature and nonlocal variables,

$$\mathbf{p} = [\mathbf{u}_I, T_I, z_I], \quad (4-1)$$

where subscript I is related to nodal quantities. In this paper the interpolation of all three fields is performed using linear shape functions N_I . The order of the interpolation in multifield problems is discussed in many papers. For example, different types of finite elements are tested in [Wcisło et al.

2013] for a case of isothermal hyperelasto-plasticity coupled with gradient damage. The research reveals that in the considered examples the elements with linear interpolation and *F-bar* enhancement preventing volumetric locking (which is discussed below) give the same results as elements with the quadratic interpolation of displacements and linear interpolation of the nonlocal variable. On the other hand, in [Simone et al. 2003] which concerns implicit gradient-enhanced continuum damage models, it is substantiated that linear interpolation of both fields (displacement vector and nonlocal variable) can be used. The provided reasoning can also be applied to the case of thermomechanical coupling, and therefore linear interpolation of temperature and displacements is admissible.

For the sake of consistency with the approach convenient for the *Ace* packages, a potential for each governing equation is introduced [Korelc 2008]. For the balance of linear momentum this potential is the Helmholtz free energy function ψ (for detailed explanation see [Korelc 2009]), the specific form of which is presented in Section 3B.

The potential for the second governing equation is proposed in the form

$$\Pi_{en} = \frac{1}{2} \frac{c}{\Delta t} (T - T_n)^2 + \frac{1}{2} k \nabla T \cdot \nabla T - \mathcal{R}T. \quad (4-2)$$

It is derived from the weak form of the energy balance (3-29) in such a way that the variation of Π_{en} is zero. The potential presented in (4-2) is valid provided that quantities k , c and \mathcal{R} are independent of temperature. However, it can be observed that \mathcal{R} , which includes plastic heating in accordance with (3-26), does not satisfy this requirement. To solve this problem without changing potential (4-2), an AD exception has been applied, i.e., additional information has been introduced into the AD process to obtain the proper derivative code [Korelc 2009]. Justification of this approach can be found in [Wcisło and Pamin 2016].

Finally, the potential for the averaging equation derived from the weak form (3-30) is proposed,

$$\Pi_z = \frac{1}{2} ((z - \kappa)^2 + l^2 \nabla_0 z \cdot \nabla_0 z). \quad (4-3)$$

Therefore, the Gauss point contribution to the element residual vector \mathbf{R}_G appearing in (2-2) consists of three parts,

$$\mathbf{R}_G = \left[\frac{\partial \psi}{\partial \mathbf{u}_I}, \frac{\partial \Pi_{en}}{\partial T_I}, \frac{\partial \Pi_z}{\partial z_I} \right], \quad (4-4)$$

and the tangent matrix is computed using (2-3).

As has been mentioned in Section 3C, the Huber–Mises–Hencky yield function is a volume-preserving plasticity model and the numerical results can be affected by the spurious effect of volumetric locking. There are two solutions to prevent such misrepresentation of the results: the first is to increase the interpolation order (which can cause a significant growth in the number of degrees of freedom and computational costs) and the second is to upgrade the finite elements using a chosen methodology as the enhanced assumed strain [Simo and Rifai 1990], selective integration or the B-bar method [Hughes 1980]. In this work the *F-bar* approach of de Souza Neto et al. [2008] has been applied. The method involves replacing the deformation gradient \mathbf{F} with its modified counterpart $\bar{\mathbf{F}}$. The formulation is based on a multiplicative split of the deformation gradient into its volumetric and isochoric parts,

$$\mathbf{F} = \mathbf{F}_{iso} \mathbf{F}_{vol}, \quad (4-5)$$

where

$$\mathbf{F}_{\text{iso}} = J^{-1/3} \mathbf{F}, \quad \mathbf{F}_v = J^{1/3} \mathbf{I}. \quad (4-6)$$

The modified deformation gradient $\bar{\mathbf{F}}$ for a selected Gauss point is computed using the isochoric part calculated at this integration point and the volumetric one derived at the centroid of the finite element.

5. Numerical tests

In this section the numerical examples simulating the response of a modeled material are presented. All computations were performed for a rectangular plate in tension in the plane strain regime.

The isothermal model is tested first with attention focused on the influence of the internal length scale on the material response and on the significance of element enhancement preventing the locking phenomenon.

The fully coupled thermomechanical model is subsequently tested for different values of the heat conduction coefficient and compared with the outcome of the model without temperature-dependence.

5A. Test parameters. The tested specimen is a plate of dimensions: $L = 0.20$ m, $W = 0.10$ m, $H = 0.0025$ m with a square imperfection in the center ($L_{\text{imp}} = 0.005$ m). Due to the symmetry of the specimen, only one quarter of the plate is considered. The imperfection is assumed as the decrease of the initial yield stress to $\sigma_{y0,\text{imp}} = 0.8\sigma_{y0}$, and for simulations with the thermomechanical coupling an increase of the thermal softening coefficient to $H_{T,\text{imp}} = 1.05H_T$ is adopted additionally, see [LeMonds and Needleman 1986]. The material parameters used in the simulations are presented in Table 1. The upper part of the table is related to the isothermal model whereas the lower part refers to the thermal coupling. Two nonzero values of the internal length parameter are assumed. The first one $l = 0.0025$ m is equal to the plate thickness and the dimension of the imperfection in the relevant quarter of the plate. The plane strain conditions are applied (displacements at all nodes in the thickness direction are restrained) and the remaining mechanical boundary conditions are assumed in such a way as to allow deformation in the width direction. The enforced maximum displacement in the length-direction is equal to $u_{\text{max}} = 0.04$ m and it is achieved after 1 s in adaptive steps.

For the coupled thermomechanical model, the whole sample is insulated, i.e., homogeneous Neumann boundary conditions are adopted on the whole surface. However, convection on the surface can also be considered, as in [Wcisło and Pamin 2016], where aspects of the convection implementation within *AceGen* are discussed.

The numerical model is generated using hexahedral elements and two finite element discretizations are used: 800 (mesh 1) and 3200 (mesh 2) elements, see Figure 1.

5B. Plate in tension in isothermal conditions. At the beginning the simulations are performed for the isothermal conditions. In the first test, the response of the sample is modeled with standard hexahedral elements with linear interpolation of both fields (displacements and the nonlocal variable), and no enrichment preventing the locking phenomenon is used.

Figure 2 presents the sum of reactions vs. load multiplier. It can be observed that all results for mesh 1 and mesh 2 coincide to a certain point in the post peak regime. When the load multiplier reaches the value 0.48, the diagrams become distinct. The value of the internal length scale does not influence the results much, and the outcomes of simulation using mesh 2 are very close to one another for each value of l .

property	symbol	value	unit
bulk modulus	K	$164.2 \cdot 10^9$	N/m ²
shear modulus	G	$80.19 \cdot 10^9$	N/m ²
initial yield stress	σ_{y0}	$0.45 \cdot 10^9$	N/m ²
residual yield stress	$\sigma_{y\infty}$	$0.6 \cdot 10^9$	N/m ²
hardening modulus	H	$129 \cdot 10^6$	N/m ²
saturation coefficient	δ	16.93	–
ductility	β	1	–
internal length	l	0, 0.0025, 0.005	m
density	ρ	$7.8 \cdot 10^3$	kg/m ³
conductivity	k	0, 100	J/(sKm)
heat capacity	c	460	J/(kgK)
thermal expansion coefficient	α_T	$12 \cdot 10^{-6}$	1/K
thermal softening modulus	H_T	0.002	1/K
dissipation heat factor	χ	0.9	-
reference temperature	T_0	273.15	K

Table 1. Material parameters.



Figure 1. Finite element discretizations of plate in tension: mesh 1 (left) and mesh 2 (right); imperfection marked with red color.

The deformed meshes with the plastic strain measure distribution at the end of the deformation process are depicted in Figures 3 and 4. It can be noticed that the localization has the form of a neck rather than shear band and can be described as a diffuse mode. This is also consistent with the force-displacement diagram in the post peak regime and the little influence of the internal length on the results. Also the differences in deformations and plastic strain distributions for two values of internal length $l = 0$ and $l = 0.005$ m for both discretizations are minor. As expected, a smoother distribution of plastic strain is observed for the nonzero value of l . In fact, the results are slightly different for the adopted meshes, the introduction of the internal length scale does not prevent the results from being discretization-sensitive.

The next simulations are performed for a model with the finite element enrichment F -bar. Figure 5 shows the load-displacement relation for the nonlocal model with different values of the internal length scale. Similarly to the previous test, the curves overlap up to the value of the displacement multiplier equal to $\lambda = 0.48$ and subsequently diverge. However, in this case the internal length has a strong influence on the mesh-insensitivity, for the higher value the diagrams for mesh 1 and mesh 2 are very close, and they suggest a localized mode of deformation, which is confirmed in Figures 6 and 7, where

shear bands are shown. It can be noticed that for the local model the strains localize in two rows of elements. The application of the gradient enhancement (see Figure 7) prevents the results from being affected by this pathological mesh-dependency and has a regularizing effect. To sum up, it is interesting that the choice of the kind of finite element has such strong influence on the results, which differ not only quantitatively but qualitatively as well.

The results obtained with the use of the finite elements with and without F -bar enrichment are compared in Figure 8 for the zero internal length scale. It was expected that the response of the material simulated with elements without enhancement would be stiffer, yet this has been confirmed only in the post peak regime.

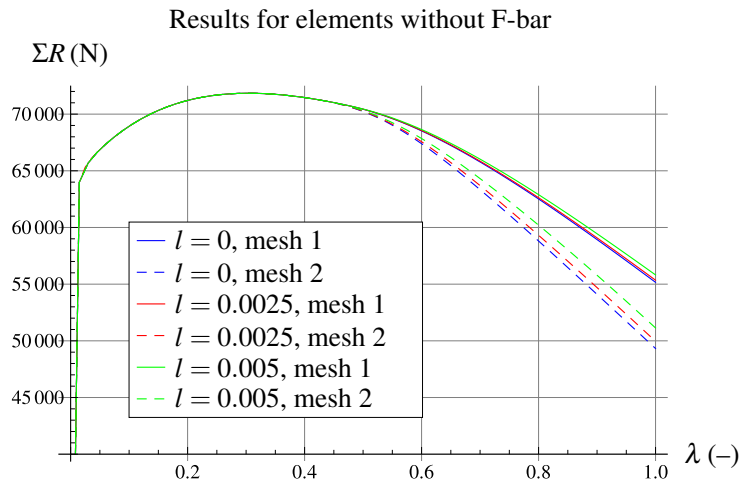


Figure 2. The sum of reactions vs. displacement multiplier (isothermal model).

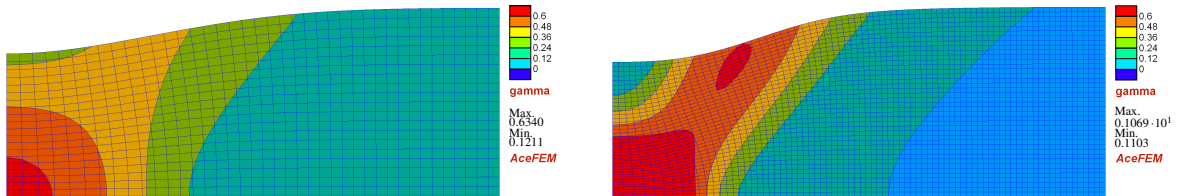


Figure 3. Deformed mesh with plastic strain measure γ distribution for mesh 1 (left) and mesh 2 (right) — isothermal model, $l = 0$, elements without F -bar enhancement.

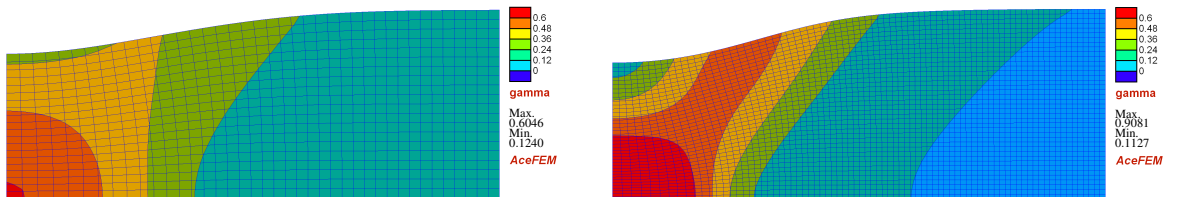


Figure 4. Deformed mesh with plastic strain measure γ distribution for mesh 1 (left) and mesh 2 (right) — isothermal model, $l = 0.005$ m, elements without F -bar enhancement.

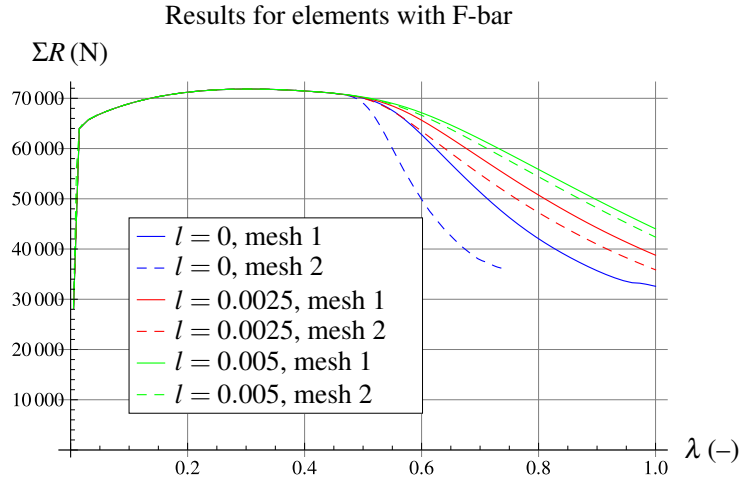


Figure 5. The sum of reactions vs. displacement multiplier (isothermal model).

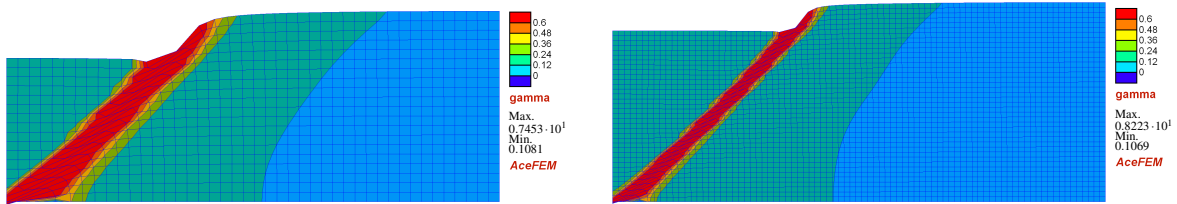


Figure 6. Deformed mesh with plastic strain measure γ distribution for mesh 1 (left) and mesh 2 (right) — isothermal model, $l = 0$, elements with F -bar enhancement.

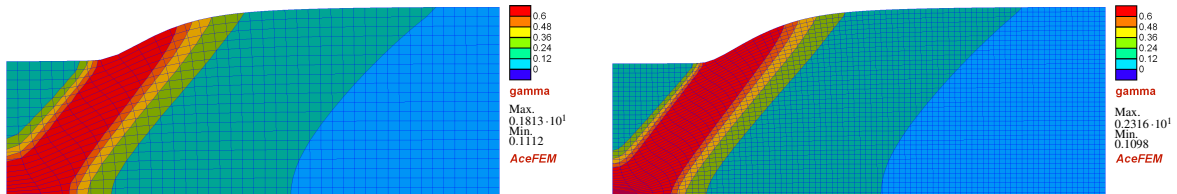


Figure 7. Deformed mesh with plastic strain measure γ distribution for mesh 1 (left) and mesh 2 (right) — isothermal model, $l = 0.005$ m, elements with F -bar enhancement.

The application of elements with F -bar enhancement causes a softer response of the material and admits a jump into a localized shear band mode, while the standard finite elements seem to prevent localization and favor the diffuse deformation. To make the matters worse, the plane strain tests (e.g., 3D ones) are as a rule more sensitive to volumetric locking, but in our test the boundary conditions are imposed in such a way that globally the plate can extend while preserving the volume. Thus, it seems that the influence of the isochoric constraint manifests itself rather at the level of shear band formation.

5C. Plate in tension simulated with thermomechanical model. In this section the coupled model is tested using material properties presented in Table 1. Apart from the two sources of instabilities which have been discussed in the previous section (geometrical and material), now the third one is going to

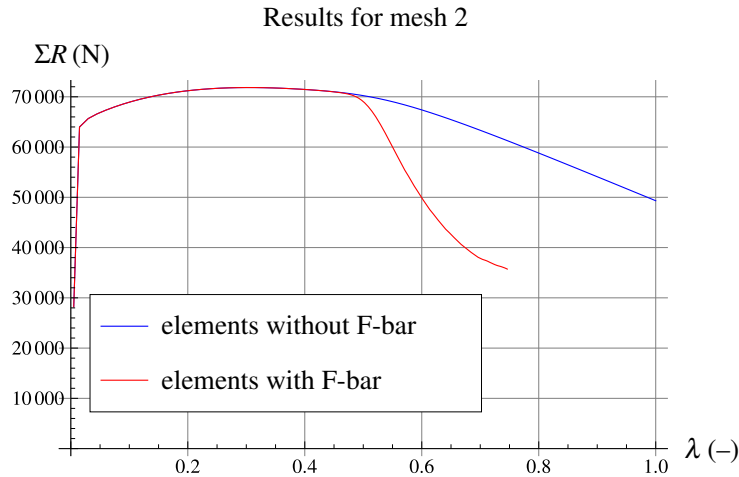


Figure 8. The sum of reactions vs. displacement multiplier (isothermal model).

be taken into account: reduction of the yield stress with temperature (thermal softening). Due to the complexity of the model and the large amount of tests which could be performed for different material and test parameters, the paper focuses solely on the presentation of the results of simulations carried out for the following cases.

First, the finite elements without F -bar are used for simulations. The results for only one value of the internal length $l = 0.005$ m are discussed due to the fact that in the isothermal case the diffuse mode was obtained and this deformation pattern (with very slight differences) is also observed for the thermomechanical coupling with different values of conductivity k and internal length l listed in Table 1.

In the next step, the elements with F -bar enrichment are tested. Here more cases are studied. We start by testing the influence of heat conduction for the model with zero internal length scale, next the effect of the internal parameter for the adiabatic case is examined, and finally the simulations are performed with two regularization effects (heat conduction and gradient averaging) included simultaneously.

5C.1. Finite elements without F -bar. The results obtained for the finite elements without enhancement are presented in Figures 9 and 10. The diagram presents the load-displacement paths for the nonlocal model with the internal length equal to $l = 0.005$ m for three cases: isothermal, adiabatic $k = 0$ and heat conduction $k = 100$ J/(sK m). The differences between these graphs are minor but the outcome for mesh 1 is stiffer than for the finer mesh. For the coarse mesh the diagrams for the adiabatic case and heat conduction coincide (red and green solid lines) so the influence of heat conduction is negligible. Also for the finer mesh that difference is insignificant.

Figure 10 presents the deformed mesh with temperature distribution. It can be observed that the presence of thermal softening does not influence significantly the shape of the deformation plot and the differences in temperature are also small.

5C.2. Finite elements with F -bar. First, the results are compared for zero internal length and different values of heat conduction to confirm that the conductivity has a regularizing effect in the absence of another length scale. The sum of reactions vs. enforced load multiplier for the analyzed cases are presented in Figure 11. It can be observed that the diagrams for heat conduction for the coarse mesh are

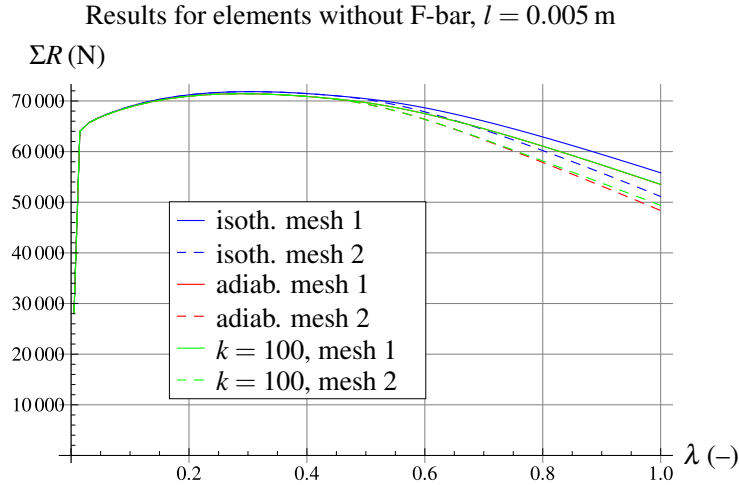


Figure 9. The sum of reactions vs. displacement multiplier.

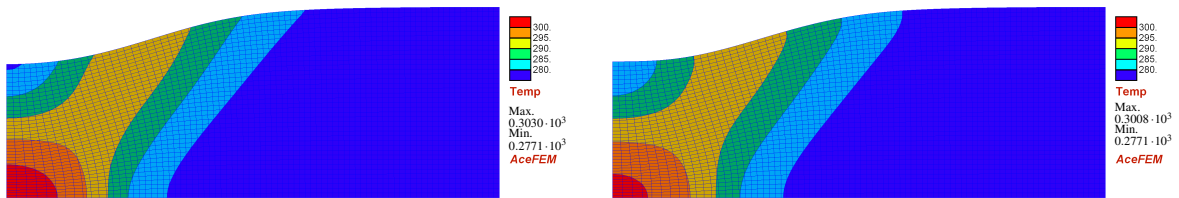


Figure 10. The deformed mesh with temperature distribution for $k = 0$ (left) and $k = 100$ J/(sKm) (right) — elements without F -bar enhancement, $l = 0.005$ m, mesh 2.

very close to the adiabatic case although some fluctuations are visible. Next, the response of the material with heat conduction was analyzed with the finer mesh. Just after the peak point the response is close to the adiabatic case, yet a convex curve is observed further on.

Figures 12 and 13 present the deformed meshes at the end of the elongation process with temperature distribution for the adiabatic case and heat conduction, respectively. As it was expected, in the first case, in which no regularization is applied the deformation is strongly localized and mesh-dependent. The generated shear band is inclined 45 degrees with respect to the longitudinal axis. However, if heat conduction is taken into account, see Figure 13, the shear band is wider but also bent. The deformations for the two considered discretizations differ slightly but have the same character — curved shear band with a narrowing in the middle of the modeled sample. When the evolution of the plastic strain measure is investigated along the line perpendicular to the initial shear band for mesh 2, it turns out that the shear band moves slightly, see Figure 14. In the first diagram we can observe a stationary shear band whereas for the case with heat conduction an evolving localization zone.

Now the influence of the internal length parameter will be examined for the adiabatic case to investigate the regularizing effect of the gradient averaging in the absence of heat conduction. Figure 15 presents the load-displacement diagrams for zero internal length scale and for $l = 0.005$ m. The results for isothermal variant are also presented for comparison. It can be noticed that the addition of thermal

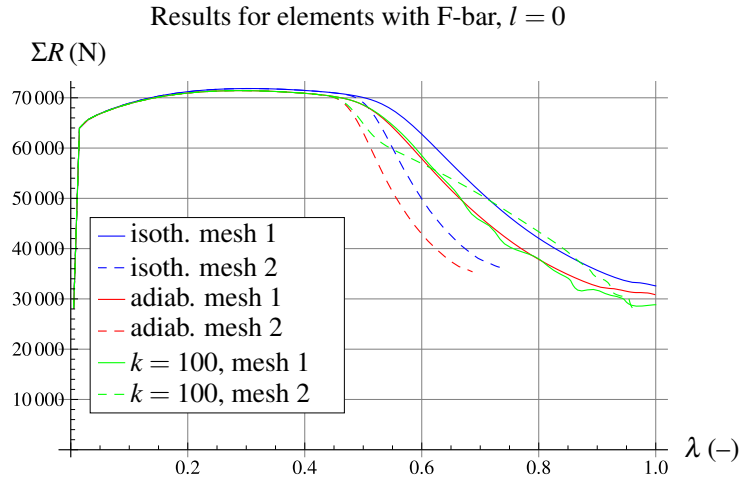


Figure 11. The sum of reactions vs. displacement multiplier.

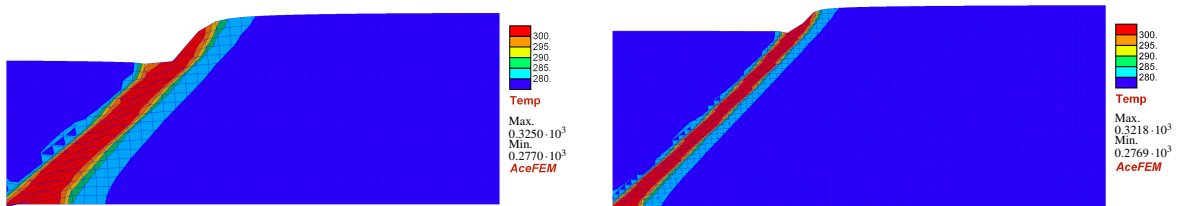


Figure 12. The deformed mesh with temperature distribution for mesh 1 (left) and mesh 2 (right) — elements with F -bar enhancement, $k = 0$, $l = 0$.

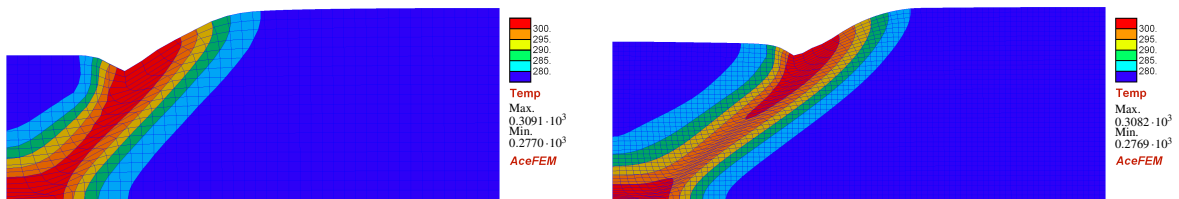


Figure 13. The deformed mesh with temperature distribution for mesh 1 (left) and mesh 2 (right) — elements with F -bar enhancement, $k = 100 \text{ J/(sKm)}$, $l = 0$.

softening indeed causes a less stiff response of the material, though its influence is stronger for the model without averaging. The diagrams showing the model with regularization are very close for each mesh and exhibit higher ductility.

Figure 16 presents the deformed meshes with temperature distribution. The response of the sample is very similar to the isothermal deformation. The shear band has a constant width and the solution does not depend on the adopted mesh.

When the results for the two regularizations (heat conduction and gradient averaging) are compared, it must be stated that, although both of them influence the discretization-dependence and increase the

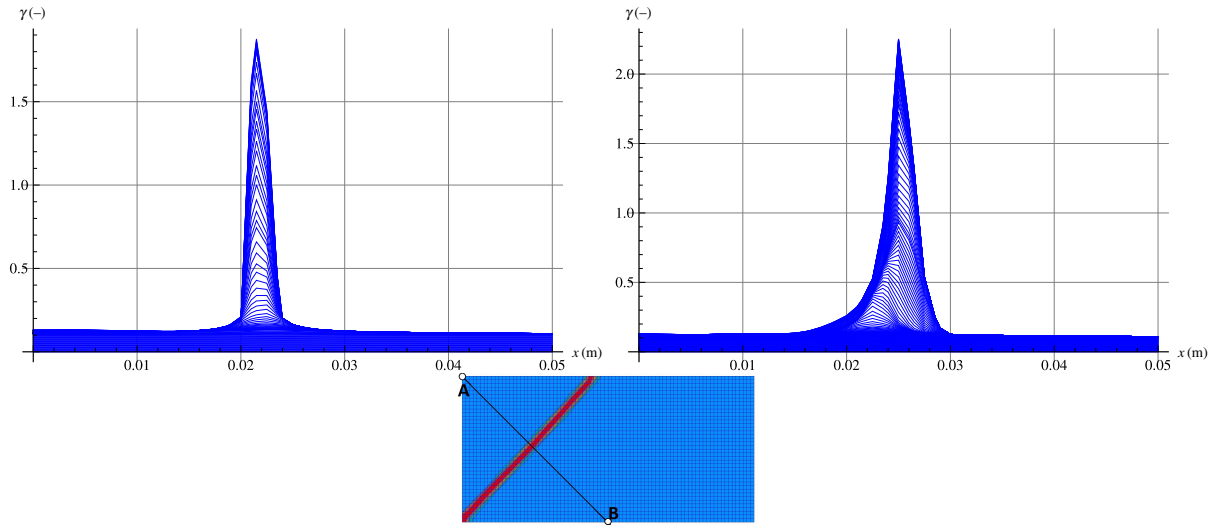


Figure 14. The evolution of the plastic strain measure γ along line A-B in reference configuration for $k = 0$ (top left) and $k = 100 \text{ J}/(\text{sKm})$ (top right) — elements with F -bar enhancement, $l = 0$.

Results for elements with F-bar, $k = 0$

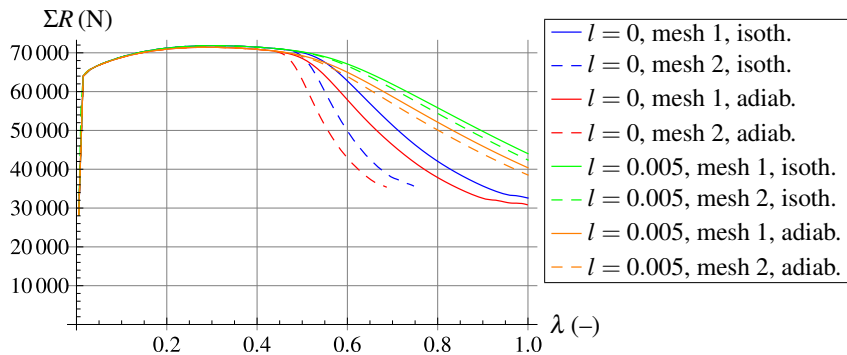


Figure 15. The sum of reactions vs. displacement multiplier.

ductility of the response, there are differences in the shape of the localization zone — the internal parameter l visibly governs the width of the band whereas for heat conduction the band has no regular form (exhibits a variable width and a curved shape).

Finally, the results of the test performed for heat conduction and gradient averaging active simultaneously are discussed. Figure 17 presents the force-displacement diagram which compares the results for two regularizations acting together (red lines) with the previous results involving only one internal length. It can be observed that the outcome is close to the response obtained for the model with gradient averaging. In this test the results for mesh 1 also exhibit fluctuations which are apparently absent in the case of finer discretization. The material modeled with gradient averaging gives a slightly softer response for mesh 2 than the model with two nonzero scales (i.e., $l = 0.005 \text{ m}$ and $k = 100 \text{ J}/(\text{sKm})$). Figure 18

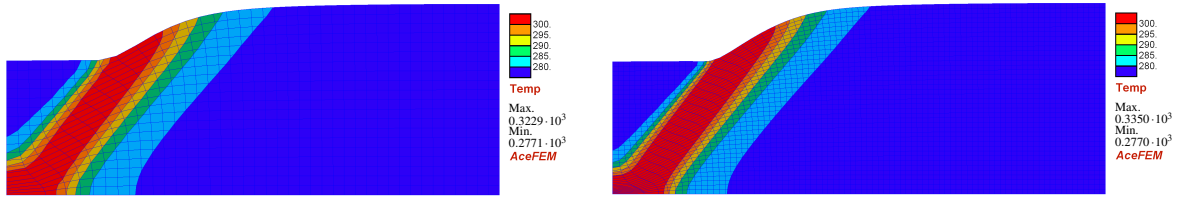


Figure 16. The deformed mesh with temperature distribution for mesh 1 (left) and mesh 2 (right)—elements with *F-bar* enhancement, $k = 0$, $l = 0.005$ m.

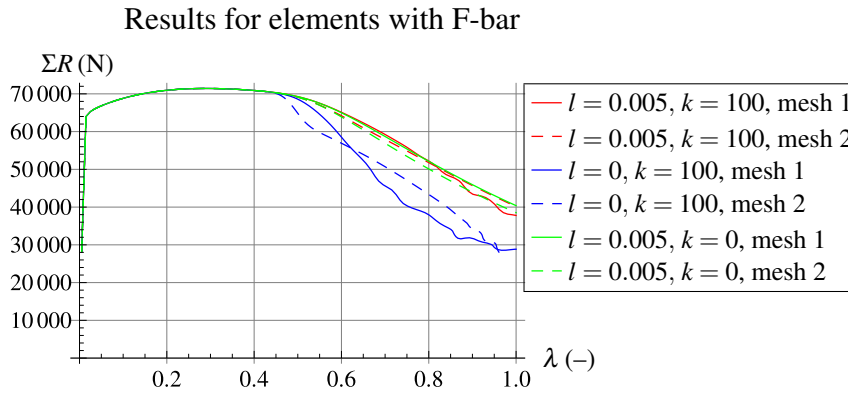


Figure 17. The sum of reactions vs. displacement multiplier for $k = 100$ J/(sKm) and $l = 0.005$ m—elements with *F-bar* enhancement.

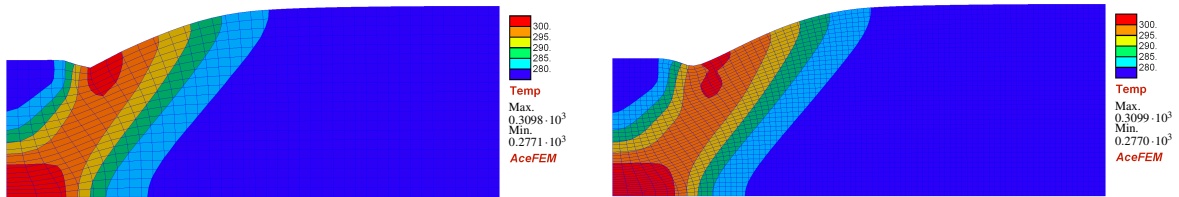


Figure 18. The deformed mesh with temperature distribution for mesh 1 (left) and mesh 2 (right)—elements with *F-bar* enhancement, $k = 100$ J/(sKm), $l = 0.005$ m.

shows the deformations of the sample for two discretizations. The results are similar for both meshes and it can be observed that the shear band width is governed by the internal length scale, but it is also bent due to heat conduction. When the diagram presented in Figure 19 is analyzed, it turns out that the band also evolves.

6. Conclusion

This paper presents an analysis of the nonisothermal large-strain model of hyperelasto-plasticity with the yield strength degradation due to damage-like variable. The thermomechanical coupling, apart from thermal expansion and plastic heating, introduces also thermal softening as the third source of the loss of stability alongside the geometrical and material effects. To prevent the pathological mesh-dependence of simulation results, gradient averaging is incorporated in the model. This treatment introduces the internal

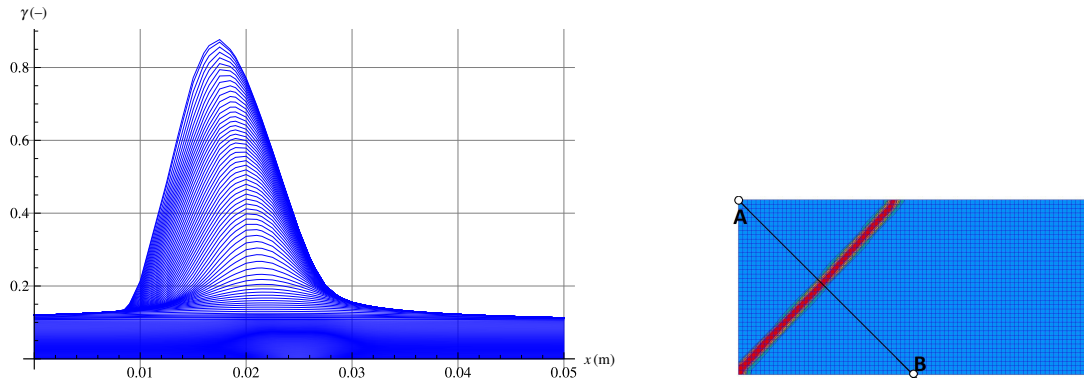


Figure 19. The evolution of the plastic strain measure γ along line A-B in reference configuration for $k = 100 \text{ J}/(\text{sKm})$ and $l = 0.005 \text{ m}$ — elements with F -bar enhancement.

length parameter which influences the ductility of the material response and the width of the shear band. Furthermore, heat conduction in the coupled thermomechanical model also has regularizing properties for the nonadiabatic case.

The developed model was implemented within FEM and tested using the elongated rectangular plate in plane strain conditions. The aims of the numerical analysis of the presented model were to examine the influence of the incorporated localization limiters on the simulation results and, moreover, to investigate how the results depend on the adopted finite elements with or without the enhancement preventing the locking phenomenon which might be encountered in a volume-preserving plasticity model.

Firstly, the isothermal analysis was carried out for different meshes, finite elements and values of the internal length scale. Although the volume-preserving plasticity was implemented, the results do not differ for the finite elements with and without F -bar enhancement in the plastic regime prior to strain localization. However, for the simulations with the finite elements without enrichment the response in the post peak zone has a diffuse form, practically independent of the internal length scale, whereas the F -bar enhancement involves strong localization of strains in a shear band. In the latter case the gradient averaging significantly influences the ductility of the material response removes the mesh-dependence.

The next step involved taking into account the nonisothermal model. The behavior of the sample simulated using the finite elements without F -bar enhancement is similar to the response in the isothermal conditions. What is more, the results actually do not depend on heat conduction. On the other hand, the response of the plate in tension modeled with the enriched elements exhibits the localized form of deformation, strongly discretization-dependent in the absence of regularization. The application of gradient averaging influences the shear band width whereas the heat conduction produces an irregular and evolving localization zone (with a changeable width and a curved shape). Thus, although both heat conduction and gradient averaging have regularizing properties, they affect deformation in different manners. The simultaneous presence of the heat conduction and gradient regularization results in the combination of these two effects.

Comparison of the obtained results shows that incorporation of finite element enhancement to avoid volumetric locking influences strongly the post peak behavior of the material, and its absence can prevent the localized form of deformation.

Finally, it is worth emphasizing the significance of the programming environment applied for the numerical treatment of the complex model. The package *AceGen*, involving automatic differentiation, is a convenient tool which allows researchers to focus on the model development and its examination instead of analytical derivation and programming.

To sum up, the new developments in the paper are:

- thermomechanical extension of the hyperelasto-plastic model including yield stress degradation and gradient averaging of the plastic strain measure,
- development of the algorithms for the symbolic-numerical tool *AceGen* based on the potential approach and performing automatic linearization of the governing equations,
- investigation of the influence of the finite element enhancement called *F-bar*, preventing the volumetric locking phenomenon on the results of the numerical simulations of shear band instability,
- analysis of the regularizing effects produced by heat conduction as well as gradient averaging and of the behavior of the sample in the simultaneous presence of two internal length parameters.

References

- [Abeyaratne and Knowles 1999] R. Abeyaratne and J. K. Knowles, “On the stability of thermoelastic materials”, *J. Elasticity* **53**:3 (1999), 199–213.
- [Aifantis 1992] E. C. Aifantis, “On the role of gradients in the localization of deformation and fracture”, *Int. J. Eng. Sci.* **30**:10 (1992), 1279–1299.
- [Areias et al. 2003] P. M. A. Areias, J. C. de Sá, and C. C. ao António, “A gradient model for finite strain elastoplasticity coupled with damage”, *Finite Elements in Analysis and Design* **39**:13 (2003), 1191–1235.
- [Batra and Kim 1991] R. C. Batra and C. H. Kim, “Effect of thermal conductivity on the initiation, growth and bandwidth of adiabatic shear bands”, *Int. J. Eng. Sci.* **29**:8 (1991), 949–960.
- [Belytschko and Lasry 1989] T. Belytschko and D. Lasry, “A study of localization limiters for strain-softening in statics and dynamics”, *Comput. Struct.* **33**:3 (1989), 707–715.
- [Benallal and Bigoni 2004] A. Benallal and D. Bigoni, “Effects of temperature and thermo-mechanical couplings on material instabilities and strain localization of inelastic materials”, *J. Mech. Phys. Solids* **52**:3 (2004), 725–753.
- [Benallal and Marigo 2007] A. Benallal and J.-J. Marigo, “Bifurcation and stability issues in gradient theories with softening”, *Modelling Simul. Mater. Sci. Eng.* **15**:1 (2007), S283–S295.
- [Bigoni 2012] D. Bigoni, *Nonlinear solid mechanics: bifurcation theory and material instability*, Cambridge University Press, 2012.
- [de Borst and Mühlhaus 1992] R. de Borst and H.-B. Mühlhaus, “Gradient-dependent plasticity: formulation and algorithmic aspects”, *Int. J. Num. Methods Eng.* **35**:3 (1992), 521–539.
- [de Borst et al. 1993] R. de Borst, L. Sluys, H. Mühlhaus, and J. Pamin, “Fundamental issues in finite element analyses of localization of deformation”, *Eng. Comput.* **10**:2 (1993), 99–121.
- [de Souza Neto et al. 2008] E. de Souza Neto, D. Peric, and D. Owen, *Computational methods for plasticity: theory and applications*, Wiley, Chichester, England, 2008.
- [Dunwoody and Ogden 2002] J. Dunwoody and R. Ogden, “On the thermodynamic stability of elastic heat-conducting solids subject to a deformation-temperature constraint”, *Math. Mech. Solids* **7**:3 (2002), 285–306.
- [Duszek et al. 1992] M. Duszek, P. Perzyna, and E. Stein, “Adiabatic shear band localization in elastic-plastic damaged solids”, *Int. J. Plast.* **8**:4 (1992), 361–384.
- [Eringen 1967] A. Eringen, *Mechanics of Continua*, Wiley, New York, 1967.

- [Forest and Aifantis 2010] S. Forest and E. C. Aifantis, “Some links between recent gradient thermo-elasto-plasticity theories and the thermomechanics of generalized continua”, *Int. J. Solids Struct.* **47**:25-26 (2010), 3367–3376.
- [Forest and Lorentz 2004] S. Forest and E. Lorentz, “Localization phenomena and regularization methods”, pp. 311–371 in *Local approach to fracture* (Paris), edited by J. Besson, Ecole d’été “Mécanique de l’endommagement et approche locale de la rupture” (MEALOR), Les presses de l’école des mines de paris, 2004.
- [Geers 2004] M. Geers, “Finite strain logarithmic hyperelasto-plasticity with softening: a strongly non-local implicit gradient framework”, *Computer Methods in Applied Mechanics and Engineering* **193**:30-32 (2004), 3377–3401.
- [Geers et al. 1999] M. Geers, R. Borst, W. Brekelmans, and R. Peerlings, “Validation and internal length scale determination for a gradient damage model: application to short glass-fibre-reinforced polypropylene”, *Int. J. Solids Struct.* **36**:17 (1999), 2557–2583.
- [Haupt 2002] P. Haupt, *Continuum mechanics and theory of materials*, 2nd ed., Advanced Texts in Physics, Springer, Berlin, 2002.
- [Hill 1958] R. Hill, “A general theory of uniqueness and stability in elastic-plastic solids”, *J. Mech. Phys. Solids* **6** (1958), 236–249.
- [Holzapfel 2000] G. A. Holzapfel, *Nonlinear solid mechanics: a continuum approach for engineering*, Wiley, Chichester, England, 2000.
- [Hughes 1980] T. J. R. Hughes, “Generalization of selective integration procedures to anisotropic and nonlinear media”, *Int. J. Num. Methods Eng.* **15**:9 (1980), 1413–1418.
- [Korelc 2008] J. Korelc, *Nonlinear finite element methods*, Springer, Berlin, 2008.
- [Korelc 2009] J. Korelc, “Automation of primal and sensitivity analysis of transient coupled problems”, *Comput. Mech.* **44**:5 (2009), 631–649.
- [Korelc 2011] J. Korelc, “AceGen and AceFEM user manual”, Technical report, University of Ljubljana, 2011, Available at <http://symbtech.fgg.uni-lj.si/>.
- [Kroner and Teodosiu 1974] E. Kroner and C. Teodosiu, “Lattice defect approach to plasticity and viscoplasticity”, in *Problems of plasticity* (Leiden, Netherlands, 1972), edited by A. Sawczuk, 1974.
- [Lee 1969] E. Lee, “Elastic-plastic deformation at finite strains”, *J. Appl. Mech. (ASME)* **36**:1 (1969), 1–6.
- [Lee and Liu 1967] E. Lee and D. Liu, “Finite-strain elastic-plastic theory with application to plane-wave analysis”, *J. Appl. Phys.* **38**:1 (1967), 19–27.
- [LeMonds and Needleman 1986] J. LeMonds and A. Needleman, “Finite element analyses of shear localization in rate and temperature dependent solids”, *Mech. Mater.* **5**:4 (1986), 339–361.
- [Li and Chandra 2003] H. Li and N. Chandra, “Analysis of crack growth and crack-tip plasticity in ductile materials using cohesive zone models”, *Int. J. Plasticity* **19**:6 (2003), 849–882.
- [Lu and Pister 1975] S. Lu and K. Pister, “Decomposition of deformation and representation of the free energy function for isotropic thermoelastic solids”, *Int. J. Solids and Struct.* **11**:7 (1975), 927–934.
- [Mandel 1974] J. Mandel, “Thermodynamics and plasticity”, in *Foundations of continuum thermodynamics*, edited by J. Delgado, Macmillan, New York, 1974.
- [Menzel 2002] A. Menzel, *Modelling and computation of geometrically nonlinear anisotropic inelasticity*, Ph.D. Thesis, University of Kaiserslautern, 2002, Available at <https://kluedo.ub.uni-kl.de/frontdoor/index/index/year/2002/docId/1334>.
- [Miehe 1995] C. Miehe, “Entropic thermoelasticity at finite strains: aspects of the formulation and numerical implementation”, *Comput. Methods Appl. Mech. Eng.* **120**:3-4 (1995), 243–269.
- [Müller and Ruggeri 1993] I. Müller and T. Ruggeri, *Extended thermodynamics*, Springer Tracts in Natural Philosophy **37**, Springer, New York, 1993.
- [Peerlings et al. 1996] R. Peerlings, R. de Borst, W. Brekelmans, and J. de Vree, “Gradient enhanced damage for quasi-brittle materials”, *Int. J. Num. Methods Eng.* **39**:19 (1996), 3391–3403.
- [Peerlings et al. 2001] R. Peerlings, M. Geers, R. de Borst, and W. Brekelmans, “A critical comparison of nonlocal and gradient-enhanced softening continua”, *Int. J. Solids Struct.* **38**:44-45 (2001), 7723–7746.

- [Pérez-Foguet et al. 2000] A. Pérez-Foguet, A. Rodríguez-Ferran, and A. Huerta, “Numerical differentiation for local and global tangent operators in computational plasticity”, *Comput. Methods in Appl. Mech. Eng.* **189**:1 (2000), 277–296.
- [Pijaudier-Cabot and Bažant 1987] G. Pijaudier-Cabot and Z. P. Bažant, “Nonlocal damage theory”, *J. Eng. Mech.* **113**:10 (1987), 1512–1533.
- [Rice 1976] J. R. Rice, “The localization of plastic deformation”, pp. 207–220 in *Proceedings of the 14th international congress on theoretical and applied mechanics*, edited by W. Koiter, North-Holland Publishing Company, 1976.
- [Ristinmaa et al. 2007] M. Ristinmaa, M. Wallin, and N. Ottosen, “Thermodynamic format and heat generation of isotropic hardening plasticity”, *Acta Mech.* **194**:1-4 (2007), 103–121.
- [Rooney and Bechtel 2004] F. J. Rooney and S. E. Bechtel, “Constraints, constitutive limits, and instability in finite thermoelasticity”, *J. Elasticity* **74**:2 (2004), 109–133.
- [Rudnicki and Rice 1975] J. Rudnicki and J. Rice, “Conditions for the localization of deformation in pressure-sensitive dilatant materials”, *J. Mech. Phys. Solids* **23**:6 (1975), 371–394.
- [Simo 1988] J. C. Simo, “A framework for finite strain elastoplasticity based on maximum plastic dissipation and the multiplicative decomposition, I: Continuum formulation”, *Comput. Methods Appl. Mech. Eng.* **66**:2 (1988), 199–219.
- [Simo and Hughes 1998] J. C. Simo and T. J. R. Hughes, *Computational inelasticity*, Interdisciplinary Applied Mathematics **7**, Springer, New York, 1998.
- [Simo and Miehe 1992] J. Simo and C. Miehe, “Associative coupled thermoplasticity at finite strains: formulation, numerical analysis and implementation”, *Comput. Methods Appl. Mech. Eng.* **98**:1 (1992), 41–104.
- [Simo and Rifai 1990] J. C. Simo and M. S. Rifai, “A class of mixed assumed strain methods and the method of incompatible modes”, *Int. J. Num. Methods Eng.* **29**:8 (1990), 1595–1638.
- [Simone et al. 2003] A. Simone, H. Askes, R. Peerlings, and L. Sluys, “Interpolation requirements for implicit gradient-enhanced continuum damage models”, *Commun. Numer. Methods Eng.* **19**:7 (2003), 563–572. Errata in **20** (2004), 163–165.
- [Sluys 1992] L. Sluys, *Wave propagation, localization and dispersion in softening solids*, Ph.D. Thesis, Delft University of Technology, 1992, Available at <http://resolver.tudelft.nl/uuid:0f9b3de9-e0ec-4d9b-a42f-fcf704d5d40e>.
- [Steinmann 1999] P. Steinmann, “Formulation and computation of geometrically non-linear gradient damage”, *Int. J. Num. Methods Eng.* **46**:5 (1999), 757–779.
- [Steinmann et al. 1999] P. Steinmann, K. Runesson, and R. Larsson, “On the analysis of adiabatic strong discontinuities within thermoplastic solids”, in *IUTAM Symposium on micro- and macrostructural aspects of thermoplasticity* (Dordrecht, Netherlands), edited by O. Bruhns and E. Stein, Kluwer Academic Publisher, 1999.
- [Stojanovitch et al. 1964] R. Stojanovitch, S. Djuritch, and L. Vujoshevitch, “On finite thermal deformations”, *Arch. Mech.* **16** (1964), 103–108.
- [Taylor and Quinney 1934] G. I. Taylor and H. Quinney, “The latent energy remaining in a metal after cold working”, *Proc. Royal Soc. Lond. A* **143**:849 (1934), 307–326.
- [Thomas 1961] Y. Thomas, *Plastic flow and fracture of solids*, Academic Press, New York, 1961.
- [Tvergaard 1999] V. Tvergaard, “Studies of elastic-plastic instabilities”, *J. Appl. Mech. (ASME)* **66**:1 (1999), 3–9.
- [Vardoulakis and Sulem 1995] I. Vardoulakis and J. Sulem, *Bifurcation Analysis in Geomechanics*, Blackie Academic & Professional, 1995.
- [Wcisło and Pamin 2014] B. Wcisło and J. Pamin, “Entropic thermoelasticity for large deformations and its AceGen implementation”, pp. 319–326 in *Recent advances in computational mechanics*, edited by T. Łodygowski et al., CRC Press, London, 2014.
- [Wcisło and Pamin 2016] B. Wcisło and J. Pamin, “Local and non-local thermomechanical modeling of elastic-plastic materials undergoing large strains”, *Int. J. Num. Methods Eng.* **65** (2016).
- [Wcisło et al. 2013] B. Wcisło, J. Pamin, and K. Kowalczyk-Gajewska, “Gradient-enhanced damage model for large deformations of elastic-plastic materials”, *Arch. Mech.* **65**:5 (2013), 407–428.
- [Wriggers et al. 1992] P. Wriggers, C. Miehe, M. Kleiber, and J. C. Simo, “On the coupled thermomechanical treatment of necking problems via finite element methods”, *Int. J. Num. Meth. Eng.* **33**:4 (1992), 869–883.

- [Yang et al. 2006] Q. Yang, L. Stainier, and M. Ortiz, “A variational formulation of the coupled thermo-mechanical boundary-value problem for general dissipative solids”, *J. Mech. Phys. Solids* **54**:2 (2006), 401–424.
- [Zbib and Aifantis 1988a] H. M. Zbib and E. C. Aifantis, “On the localization and postlocalization behavior of plastic deformation, I: On the initiation of shear bands”, *Res Mechanica* **23** (1988), 261–277.
- [Zbib and Aifantis 1988b] H. M. Zbib and E. C. Aifantis, “On the localization and postlocalization behavior of plastic deformation, II: On the evolution and thickness of shear bands”, *Res Mechanica* **23** (1988), 279–292.
- [Zbib and Aifantis 1988c] H. M. Zbib and E. C. Aifantis, “On the localization and postlocalization behavior of plastic deformation, III: On the structure and velocity of Portevin–Le Chatelier bands”, *Res Mechanica* **23** (1988), 293–305.

Received 1 Mar 2016. Revised 17 Jun 2016. Accepted 31 Aug 2016.

JERZY PAMIN: jpamin@L5.pk.edu.pl

Institute for Computational Civil Engineering, Cracow University of Technology, ul. Warszawska 24, 31-155 Kraków, Poland

BALBINA WCISŁO: bwcislo@L5.pk.edu.pl

Institute for Computational Civil Engineering, Cracow University of Technology, ul. Warszawska 24, 31-155 Kraków, Poland

KATARZYNA KOWALCZYK-GAJEWSKA: kkowalcz@ippt.pan.pl

Institute of Fundamental Technological Research, Polish Academy of Sciences, ul. Pawińskiego 5B, 02-106 Warszawa, Poland

JOURNAL OF MECHANICS OF MATERIALS AND STRUCTURES

msp.org/jomms

Founded by Charles R. Steele and Marie-Louise Steele

EDITORIAL BOARD

ADAIR R. AGUIAR	University of São Paulo at São Carlos, Brazil
KATIA BERTOLDI	Harvard University, USA
DAVIDE BIGONI	University of Trento, Italy
YIBIN FU	Keele University, UK
IWONA JASIUK	University of Illinois at Urbana-Champaign, USA
C. W. LIM	City University of Hong Kong
THOMAS J. PENCE	Michigan State University, USA
GIANNI ROYER-CARFAGNI	Università degli studi di Parma, Italy
DAVID STEIGMANN	University of California at Berkeley, USA
PAUL STEINMANN	Friedrich-Alexander-Universität Erlangen-Nürnberg, Germany

ADVISORY BOARD

J. P. CARTER	University of Sydney, Australia
D. H. HODGES	Georgia Institute of Technology, USA
J. HUTCHINSON	Harvard University, USA
D. PAMPLONA	Universidade Católica do Rio de Janeiro, Brazil
M. B. RUBIN	Technion, Haifa, Israel

PRODUCTION production@msp.org

SILVIO LEVY Scientific Editor

Cover photo: Ev Shafir

See msp.org/jomms for submission guidelines.

JoMMS (ISSN 1559-3959) at Mathematical Sciences Publishers, 798 Evans Hall #6840, c/o University of California, Berkeley, CA 94720-3840, is published in 10 issues a year. The subscription price for 2017 is US \$615/year for the electronic version, and \$775/year (+\$60, if shipping outside the US) for print and electronic. Subscriptions, requests for back issues, and changes of address should be sent to MSP.

JoMMS peer-review and production is managed by EditFlow[®] from Mathematical Sciences Publishers.

PUBLISHED BY

 **mathematical sciences publishers**
nonprofit scientific publishing

<http://msp.org/>

© 2017 Mathematical Sciences Publishers

Special issue on Coupled Field Problems and Multiphase Materials

Preface	CORINA S. DRAPACA, STEFAN HARTMANN, JACEK LESZCZYŃSKI, SIVABAL SIVALOGANATHAN and WOJCIECH SUMELKA	1
Variational methods for the solution of fractional discrete/continuous Sturm–Liouville problems	RICARDO ALMEIDA, AGNIESZKA B. MALINOWSKA, M. LUÍSA MORGADO and TATIANA ODZIJEWICZ	3
Analytical and numerical solution of the fractional Euler–Bernoulli beam equation	TOMASZ BLASZCZYK	23
Fractional calculus in neuronal electromechanics	CORINA S. DRAPACA	35
Time-adaptive finite element simulations of dynamical problems for temperature-dependent materials	MATTHIAS GRAFENHORST, JOACHIM RANG and STEFAN HARTMANN	57
Computer simulation of the effective viscosity in Brinkman filtration equation using the Trefftz method	JAN ADAM KOŁODZIEJ, MAGDALENA MIERZWICZAK and JAKUB KRZYSZTOF GRABSKI	93
Numerical simulations of mechanical properties of alumina foams based on computed tomography	ZDZISŁAW NOWAK, MARCIN NOWAK, RYSZARD PEŁCHERSKI, MAREK POTOCZEK and ROMANA ŚLIWA	107
Gradient-enhanced large strain thermoplasticity with automatic linearization and localization simulations	JERZY PAMIN, BALBINA WCISŁO and KATARZYNA KOWALCZYK-GAJEWSKA	123

